Computational geometry-based scale-space and modal image decomposition: Application to light video-microscopy imaging

Anatole Chessel, Bertrand Cinquin, Sabine Bardin, Jean Salamero, Charles Kervrann

Computational geometry-based scale-space and modal image decomposition

Application to light video-microscopy imaging

Anatole Chessel[1], Bertrand Cinquin[3,4], Sabine Bardin[3], Jean Salamero[3,5], and Charles Kervrann[1,2]

[1] INRIA Rennes
[2] INRA-MIA
[3] UMR 144 CNRS-Institut Curie
[4] Soleil Synchrotron
[5] PICT-IBiSA Institut Curie

Abstract. In this paper a framework for defining scale-spaces, based on the computational geometry concepts of α-shapes, is proposed. In this approach, objects (curves or surfaces) of increasing convexity are computed by selective sub-sampling, from the original shape to its convex hull. The relationships with the Empirical Mode Decomposition (EMD), the curvature motion-based scale-space and some operators from mathematical morphology, are studied. Finally, we address the problem of additive image/signal decomposition in fluorescence video-microscopy. An image sequence is mainly considered as a collection of 1D temporal signals, each pixel being associated with its temporal intensity variation.

1 Introduction

Vision is a complex and hierarchical process of aggregation and reconstruction going from pointwise data to global information. The scale-space approach which builds several versions of the original signal at increasingly coarser scales, is a general framework for investigating those hierarchies. In this paper we propose to explore how to derive such a scale-space from a computational geometry point of view based on space or time signal/image convexity.

To our knowledge, the tools from computational geometry [7], commonly used in images synthesis and 3D modeling, are quite unusual as far as raster images and computer vision are concerned. Typically, a 2D image may be viewed as a collection of sampled points on a surface in $\mathbb{R}^3$, and may be represented by computational geometry objects using *projection* and *interpolation* operators, as we shall see in section 2.

The notion of α-*shape* [8], which roughly corresponds to the "up-to-$\sqrt{\alpha}$-details-convex-hull" was introduced to represent 3D objects from given unorganized point clouds in $\mathbb{R}^3$. In our approach, it is applied to known objects (signals or images) to define the so-called α-*scale-space*. In some way, this modeling can

be thought of as a continuous variant of the Empirical Mode Decomposition (EMD) introduced earlier for signal decomposition in [10].

The relationships between the proposed scale-space and previous mathematical frameworks are given in section 3. The motion-by-curvature is especially examined since it constitutes a possible interpolation operator needed in our approach. An equivalence with the usual *opening* operators from mathematical morphology is also presented.

In section 4, a demonstration of the methodology applied to an usual decomposition problem in biological imaging is proposed. In some circumstances, the studied fluorescence video-microscopy sequences can be viewed as the sum of a diffusing component (slowly varying in space and time), and a very localized faster moving component. The proposed algorithm is mainly used to analyze 1D temporal signals extracted from a temporal series of images. The implementation is now routinely used by biologists and collaborators because of its rapidity of execution and its simplicity of control.

2 Computational geometry-based scale-space for curves

This section is devoted to the description of a new morphological scale-space based on the computational geometry theory and α-shape concept [8]. The theory is laid out for $\mathbb{R}^d$, but is mainly applied to signals and images, that is α-shapes in $\mathbb{R}^2$ and $\mathbb{R}^3$. An analogy with EMD is also discussed in this section.

2.1 α-shapes and convexity

The key ingredients of computational geometry (see Fig. 1), are simplices, that is points, segments, triangles and tetrahedron. Sets of simplices form complexes.

Definition 1.

- *A* k-simplex σ_T *is the convex combination of a set* T *of* $k+1$ *points in* $\mathbb{R}^d$ *(*k*-simplices are points (*$k=0$*), segments (*$k=1$*), triangles (*$k=2$*) or tetrahedrons (*$k=3$*)).*
- *A* complex K *is a set of simplices verifying: i) If* $\sigma_T \in K$, $\forall U \in T$, $\sigma_U \in K$*; ii) If* σ_U, $\sigma_V \in K$*, then* $\sigma_{U\cap V} = \sigma_U \cap \sigma_V$*.*
- *A* triangulation *of a set* P *of points in* $\mathbb{R}^d$ *is a connected complex where all the* k*-simplices are included in a* $k+1$*-simplex,* $0 \leq k < d$*.*
- *A* Delaunay triangulation *of a set* P *of points in* $\mathbb{R}^d$ *is a triangulation where the circumscribed circle of all the* d*-simplices does not include any points of* P*. The triangulation is unique if the points are in generic positions. The triangulation is a tessellation of the convex hull of* P*.*
- *A* filtration *of a complex* K *is a nested sequence of complexes included in* K*:* $\emptyset = K^0 \subseteq K^1 \subseteq \ldots \subseteq K^m = K$*.*

In Fig.1, the Delaunay triangulation of a point set is shown in blue and the original points are shown in red.

The notion of α-shape is based on Delaunay triangulations and amounts to selecting points "with enough empty space around them". More formally,

Definition 2 (α-shapes). *Let P be a set of points of $\mathbb{R}^d$ and $\mathcal{T}_P$ its Delaunay triangulation. Let σ_T be a simplex of $\mathcal{T}_P$, c_T the smallest sphere going through T and ρ_T its radius. σ_T belongs to the* α-complex *K_α of P, $\alpha \geq 0$ if and only if either of these propositions is true:*

1. *$\rho_T^2 < \alpha$ and c_T does not include any other points of P,*
2. *$\sigma_T \subset \sigma_U$ with $\sigma_U \in K_\alpha$.*

The subset of $\mathbb{R}^d$ actually covered by the α-complex (the underlying space*) is called the* α-shape *$\mathcal{S}_\alpha$ of P.*

In the general case, the α-complex is not pure, i.e. it may contain isolated points or segments not included within a triangle. Thus, the *regularized* α-shapes are also defined:

Definition 3 (regularised α-shapes). *Let P be a set of points of $\mathbb{R}^d$, $\mathcal{T}_P$ its Delaunay triangulation and K_α its α-complex, $\alpha \geq 0$. The* regularized α-complex *$\tilde{K}_\alpha$ of P is the largest complex (wrt inclusion) included in K_α for which all the k-simplices are included in a $k+1$-simplex.*
The regularized α-shape *$\tilde{\mathcal{S}}_\alpha$ is the underlying space of the regularized α-complex.*

The following basic property holds true for both the α-shapes and regularized α-shapes we have defined:

Property 1.

- There exists a finite number of values of α leading to distinct α-complexes and α-shapes.
- If $\alpha = 0$, $K_\alpha = \mathcal{S}_\alpha = P$.
- There exists a finite value α_M such that $\forall \alpha \geq \alpha_M \ K_\alpha = \mathcal{T}_P$.
- The sequence $\{K_\alpha\}$, $0 \leq \alpha \leq \alpha_M$, is a filtration of $\mathcal{T}_P$.

Intuitively, the idea is to define the "convex-up-to-$\sqrt{\alpha}$" hull of a set of points. For a given α, the α-shape consists of the points "with enough empty space around them". The resulting shape is made of $\sqrt{\alpha}$ sized concavities. In Fig.1, the α-shape (for a given α) is shown in green and is a subset (according to a size criteria) of the original Delauney triangulation (in blue) computed from the initial set of points (in red).

2.2 α-scale-space framework

In this section, we use the α-shape concept to define original scale-spaces. Let $u : \mathbb{R}^n \rightarrow \mathbb{R}$ be a continuous function, $n = 1$ or 2. Let $d = n + 1$, and $P = \{(x_1, \ldots, x_n, u(x_1, \ldots, x_n)) \in \mathbb{R}^d | \ (x_1, \ldots, x_n) \in \mathbb{N}^n\}$ the finite set of points of $\mathbb{R}^{n+1} = \mathbb{R}^d$ corresponding to samples from u obtained at integer coordinates. Let $\tilde{\mathcal{P}}_\alpha, \ \alpha \geq 0$ be the regularized α-shapes of P in $\mathbb{R}^d$. Considering sampled points

in $\mathbb{R}^{n+1}$ allows us to pass from the continuous to the computational geometry setting. But going back from a computational geometry object in $(n+1)$D to a continuous function in $\mathbb{R}^n$ two tools will be needed: a *projection* operator to get something mono-valued in nD and an *interpolation* operator for continuity.

Definition 4 (lower envelope). *The lower envelope of a set of functions $H = \{H_1, \ldots, H_n\}$ defined in $R_1 \ldots, R_n \subset \mathbb{R}^n$ is the pointwise minimum over H: $\mathcal{L}_H = \min_{1<i<n} \bar{H}_i$, with $\bar{H}_i(x) = H_i(x)$ if $x \in R_i$ and $+\infty$ elsewhere (conversely, the upper envelope is defined as the pointwise maximum over H).*

The lower (upper) envelope of a complex can then be computed by associating a unique value to each vertical line, the minimal (maximal) one, thus performing a projection along the vertical axis. Hence, we define

Definition 5. *P_α^- (resp. P_α^+) is the set of points of P belonging to the lower (resp. upper) envelope of $\tilde{\mathcal{P}}_\alpha$.*

Thus, $P_\alpha^{+(-)}$ are *selective sub-samplings* of u based on local convexity analysis. By interpolating those two sets of points, we can define sets of functions corresponding to the original function analyzed at different increasing scales.

Let Ω be an open of $\mathbb{R}^n$ and $f : \partial\Omega \to \mathbb{R}$ values defined on its border. Let I be an interpolation operator that associates a unique function on Ω to f defined onto $\partial\Omega$. In what follows, I is assumed to verify the maximality principle: $\max_{\partial\Omega} f \geq \max_\Omega I(f) \geq \min_\Omega I(f) \geq \min_{\partial\Omega} f$. We can now define:

Definition 6. *Let I be an interpolation operator verifying the maximality principle. Considering a point $P = (x_1, x_2, x_3)$ as a function of $\mathbb{R}^2$ $f(x_1, x_2) = x_3$, we define the upper and lower α-scale space as: $u_\alpha^+ = I(P_\alpha^+)$ and $u_\alpha^- = I(P_\alpha^-)$. The α-scale space of u is then defined as $u_\alpha = \frac{(u^+ + u^-)}{2}$.*

In practice, various interpolation operators can be used, depending on the application. In 1D, a linear interpolation is the most usual. The question is more difficult in 2D and more details are given in the following sections. From the basic properties of α-shape explained above, basic properties of α-scale-spaces are given:

Property 2.

- For $\alpha = 0$, $u_\alpha^+ = u_\alpha^- = u_\alpha = u$.
- For $\alpha > \alpha_M$, u_α^+ and u_α^- are respectively the upper and lower convex hulls of u.
- For all α, $u_\alpha^+ \geq u \geq u_\alpha^-$.

Properties of invariance (or covariance) are also of particular interest in the case of scale-spaces. Because the α-shape is related to the distance between points, it is invariant to isometric transformations and defined up to a scale factor.

Property 3 (Invariance). u_α^+, u_α^- and u_α are invariant to similarity in $\mathbb{R}^d$.

This includes rotation and translation (for images), gray level shift and contrast inversion. On the other hand, invariance to generic or even increasing contrast changes does not hold. Indeed such a transformation would treat one direction independently from the others and thus would break the isotropy of the underlying algorithms. It is worth noting that it might be possible to exhibit more invariance properties by formulating the computational geometry framework using other metrics, but this is out of the scope of this paper.

2.3 Relationships with the Empirical Mode Decomposition

The EMD algorithm was introduced for highly non-stationary and non-linear 1D physical signals by Huang in [10], and since extended to 2D images [11]. A modal decomposition of signals is obtained by applying an iterative and intuitive algorithm which received recently a more formal justification within the wavelet framework [9].

Briefly, the EMD algorithm is composed of two loops. In the inner loop, the upper and lower envelopes are iteratively computed based on an interpolation process of maxima and minima and further used to build a "mean envelope". The difference between the "mean envelope" and the signals yields a component, called the IMF (Intrinsic Mode Function) and a residual signal with no high frequency. The computation of the "mean envelope" and subtraction are iterated in the outer loop until the residual is a monotonic trend. Ultimately, we have

$$u \;=\; \sum_{i=1}^{n} c_i + r$$

where the $\{c_i\}$ represent the modes that capture increasingly higher frequencies, and r represents the residual component. In the terminology of scale-spaces, we rather write

$$u_k \;=\; u - \sum_{i=1}^{k} c_i,\;\; k = [1 \dots n]$$

with $u_0 = u$ and $u_{n+1} = r$ by convention, to yield an increasingly coarse description of the original signal. Thus EMD can be seen as a discrete scale-space or, as the number of modes is relatively small, a scale-space with a limited number of scales automatically selected.

Our proposed α-scale-space is consistent with this framework. The common ideas are modes corresponding to variations around a local mean, and local maxima/minima used to compute upper and lower envelopes. Nevertheless, they differ for two reasons: i) the more continuous nature of the α-shape decomposition,which consider a larger number of modes and scales; ii) the possibility of computing non-symmetric modes with the α-shapes. The IMFs computed by EMD are symmetric components with respect to the computed mean, which was desired in [10]. In image analysis, since the images are lower bounded, this constraint can be relaxed. The relationships between our scale-space formulation and the modal decomposition outlined by EMD however is worth keeping in mind. Section 4 illustrates these connections, especially if we consider lower α-scale-spaces.

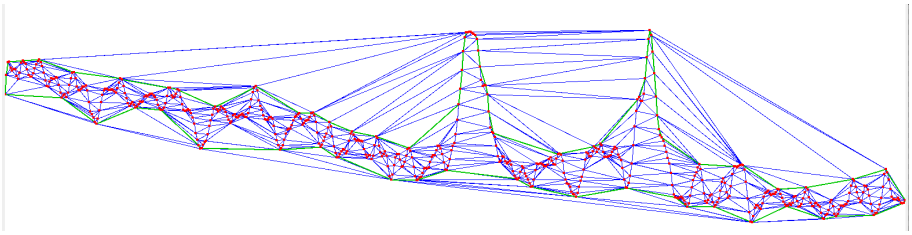

Fig. 1. Intensity variation wrt time (for a given pixel) in video-microscopy (see section 4). Red: original points (see also Fig. 4), blue: Delauney triangulation, green: α-shapes.

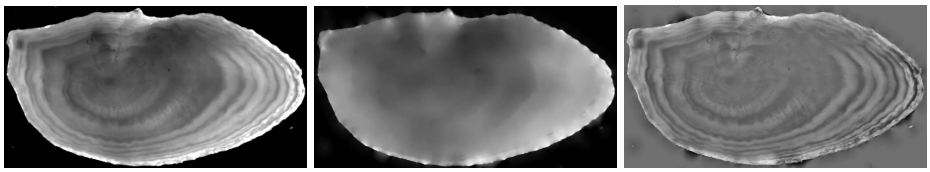

Fig. 2. Example of α-scale-space applied to a 2D otolith image (see text). Left to right: original, α-scale-space for $\alpha = 100$, image difference.

2.4 Implementation and first examples

In the following, the CGAL implementation of the computational geometry algorithms is used [2]. In the 1D case, a simple linear interpolation is performed. For 2D images, the interpolation is more problematic and a scattered points interpolation framework must be considered (see [1, 6] for reviews). Natural neighbor interpolation [3] is used, as is it defined in the same computational geometry framework available in CGAL. Other possible choices are discussed in the next section.

Figure 1 shows a 1D example in video-microscopy, i.e. the intensity variations for a given pixel wrt time (see section 4 for details). The two peaks, corresponding to two objects passing through that pixel, are of interest. This illustrates the Delauney triangulation of a set of points and its relationships with the α-shape concept. The lower α-scale-space is defined as the green curve below the red points. Thus the difference with the original curve allows us to recover the peaks.

Figure 2 shows a 2D example of the α-scale-space decomposition when applied to an otolith image. Otoliths are biological hard tissue (of few mm [12]) of much use in marine biology and ecology. The α-scale-space corresponds to the trend in intensity, while the difference between the trend and the original image corresponds to variations around that trend.

3 Interpolation and α-shapes: mean curvature motion and mathematical morphology

As defined, the α-scale-space is based on selective sub-sampling and interpolation. In this section, we investigate several interpolation operators. The so-called

mean curvature motion and some tools from the *mathematical morphology*, are mainly studied.

3.1 α-shape and curvature motion

Motion-by-curvature is a partial differential equation (PDE) commonly-used in image analysis. Curves evolve with a speed and a direction depending on the local curvature. If an image is represented as a stack of non-intersecting level lines, each level line evolves according to its own curvature. It is established that evolving an image according to the mean curvature motion amounts to minimizing the total variation of the image. Finally, an image is also a 3D surface and may be deformed according to its local curvatures in $\mathbb{R}^3$.

In [6] an axiomatic approach for image interpolation was studied, singling out three second order interpolation operators: *i)* the first operator is the *Laplacian* operator, known not to be able to handle isolated data points and thus not suitable to scattered point interpolation; *ii)* the second operator is the *Absolutely Minimizing Lipschitz Extension* (AMLE) which supposes a Lipschitz initialization and thus not suitable to scattered point interpolation either; *iii)* the third operator is the *curvature* operator for which, when used as an interpolation operator, neither uniqueness nor existence of solutions holds.

In [16], L. Vese proposed a mean curvature motion based on PDEs for the computation of convex hulls of signals and images, and proved existence and uniqueness of viscosity solutions:

$$\begin{cases} \dfrac{\partial u}{\partial s} = \sqrt{1+|Du|^2}\,\min(0, \lambda_{min}(D^2u)), \\ u(x,0) = u, \end{cases}$$

where $\lambda_{min}(D^2u)$ is the lower eigenvalue of the Hessian matrix. It is an alternative way of computing a convexity based scale-space, yielding a family of functions of increasing convexity up to the convex hull. Two flows, converging respectively toward the convex and concave hulls, are then defined. These flows can be used in a similar way as the upper and lower α-scale- spaces defined earlier, that is two envelopes enclosing the original function. However the relationships between the two frameworks cannot be easily exhibited.

In the particular case of a convex function u, the PDE can be used as an interpolation operator of P_α^-. It amounts to using the convex hull of P_α^-. A tessellation of u into convex components would be needed in the general case.

3.2 α-shape and mathematical morphology

Pioneered by Serra and Matheron, the mathematical morphology [15] is one of the most classical theory in image analysis. In the scale-space theory, it has been shown to be related to the mean curvature motion and related filters [5].

Typically the *gray-scale opening* of an image is defined as the composition of a gray-scale *erosion* and *dilation*. Let u be considered as the part of $\mathbb{R}^d$ below it

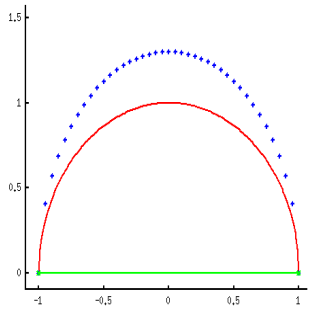

Fig. 3. Lower α-scale-space and *opening* on an artificial example (see text). Blue crosses: original points; red line: *opening* by a disk of radius 1; green: α-scale-space for $\alpha = 1$

(in $\mathbb{R}^3$ for images: $u = \{x \in \mathbb{R}^3 |\ x_3 < u(x_1, x_2)\}$). Its opening can be written as:

$$O(u) = \text{Sup}\{B \subset \mathcal{B},\ B \subset u\}$$

with $\mathcal{B}$ the class closed under union generated by a structuring element B_0. Thus if the structuring element B_0 is a ball of radius r, $O_r(u)$ is the best approximation of u below u by unions of ball in $\mathbb{R}^3$. It corresponds to the so-called *"rolling ball" algorithm* commonly used to remove backgrounds and trends in biological imaging. It is intuitively related to the α-shape, as both are obtained through an approximation by "sweeping balls". Indeed we have

Proposition 1. *There exists an interpolation operator I for which u^+_α and u^-_α are respectively the morphological opening and closing of u by a sphere of radius $\sqrt{\alpha}$.*

Proof. Let $P^-_\alpha = \{(x^i_1, \ldots, x^i_d), i = 1 \ldots |P^-_\alpha|\}$. Points in P^-_α have by definition an empty space of radius $\sqrt{\alpha}$ below them, so we can write

$$\forall i \in [1 \ldots |P^-_\alpha|],\ O_{\sqrt{\alpha}}(u)(x^i_1, \ldots, x^i_{d-1}) = x^i_d,$$

that is all points of P^-_α are in $O_{\sqrt{\alpha}}(u)$. Thus $u^-_\alpha = O_{\sqrt{\alpha}}(u)$ is a valid definition of a lower α-scale-space. The same ideas apply for closing and upper α-scale-spaces.

However, the resulting interpolation operator does not verify the maximality principle. It can be seen on a simple counter-example: let $b : [-1, 1] \to \mathbb{R}$ be the half-sphere of radius 1 centered on O, and let $u = b + \varepsilon b$, with ε small. Then the opening with a ball of radius 1, $O_1(u) = b$, while P^-_α for $\alpha = (1)^2$ is the points $(0, -1)$ and $(0, 1)$. As an interpolation of P^-_α in $[-1, 1]$, $O_1(u)$ does not verify the maximality principle. This example is presented in Fig.3 where u is shown in blue and r corresponding to the opening and the interpolated α-scale-space are respectively shown in red and green.

Thus the connection with some tools from mathematical morphology gives an intuitive idea of α-scale-space, but is not a suitable choice in practice since the maximality principle does not hold.

4 Application to additive signal decomposition in fluorescence video-microscopy

The proposed framework is especially used to solve the additive signal decomposition problem in fluorescence microscopy. We shall see that the proposed framework is particularly adapted to process such image sequences depicting two components with different spatio-temporal characteristics that translate into signals with different convexities.

Biological context and motivation. The discovery of the xFP (naturally fluorescent proteins), for which the 2008 chemistry Nobel prize was awarded, along with advances in genetic engineering allow for the coupling of any protein of interest with a fluorescent tag in cells, tissues and organisms. Dynamic visualization of *in vivo* protein behavior is then possible in many biological models. In this section, we study the Rab GTPase family, a family of proteins involved in the intra-cellular transport and maintenance of membranes.

The Rab proteins are known to exist in two main states, a cytosolic state slowly diffusing and a membrane state in which they eventually move as vesicles with directed movements. The fluorescence depends in first approximation on the concentration of fluorescent proteins, and the membrane state consists of vesicles of much higher concentration than the cytosol in which they are embedded. Thus the vesicles are seen as dots of higher intensity moving rather quickly on a slowly varying background.

The separation of those two components is a necessary step for several studies [13]. Thanks to the biophysical properties of the image, it can be regarded as an additive signal decomposition problem. The intensity of a given pixel is proportional to the total concentration of the proteins in the corresponding volume, defined as the sum of the concentration of the proteins in each state. Thus for an acquired image sequence u, we can write $u = u_{cyt} + u_{ves}$ with u_{cyt} the cytosol component slowly varying in both space and time, and u_{ves} the vesicular component, very localized in space and time and moving rather quickly.

In our experiments, we performed pairwise comparisons of the behavior of specific Rab complexes. Rabin8 against Rab8wt (wild type) or against Rab11Awt are especially studied in this paper. Rabin8 was previously shown to interact with both (or either) the two Rab GTPases, Rab8 and Rab11A, whose functions in membrane traffic are closely related, although separated in time and location. Those proteins have clear different properties, and in particular show different separations into membrane and cytosolic states. The images shown are taken using fast Total Internal Reflection Fluorescent microscopy (10 to 20 frames/seconds, time sequences 120s) which allows for an imaging of the very narrow depth inside the cell near the plasma membrane.

Experiments and results. Previous related works include spatial detection using wavelets [14] and background extraction using a temporal model [4]; the vesicles appear as bright blobs in space or as spikes in time. Figure 4 shows the

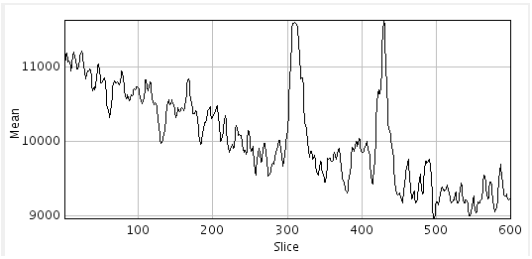

Fig. 4. Intensity variation wrt time for a given pixel (the two spikes correspond to two vesicles passing through that pixel).

intensity variation wrt time for a given pixel (the two spikes correspond to vesicles passing through that pixel). Generally, the decreasing trend corresponding to the loss of fluorescence over time (known as observational photobleaching) needs to be estimated and to be potentially removed. Our scale-space framework is then particularly well suited if we consider the lower envelope as the key feature to analyze such additive signals.

When applied to individual 2D images, the image sequence decomposition is not reliably performed (not shown in the paper). The typical size of vesicles is relatively small and may be confounded by noise. It turns out that the temporal characteristics (movements, apparition and disappearance) are actually more pregnant than the spatial ones, and are analyzed further.

Figure 5 shows the application of the proposed lower α-scale-space to analyze 1D temporal signals, processed individually. Two typical sequences depicting several Rab proteins are presented. We decided arbitrarily to display the maximum intensity projection (MIP) along the time axis since these maps enable to summarize the sequence contents (the videos are more demonstrative but can not be embedded in the paper). In Fig.5, the bright lines correspond to the main trajectories of moving vesicles. The MIP maps of the original image sequences are shown on the first row in Fig. 5. The second and the third rows show respectively the MIPs of the vesicular components and the MIPs of computed trends corresponding to the lower α-scale-spaces when $\alpha = 1000$. The vesicular components are computed as the difference between the original image sequence and its computational geometry-based scale-space representation. By summing the two decomposed image sequences, we get the original image sequences with no loss of information. Clearly, the bright lines are enhanced and the slowly moving background contain no blob (moving vesicles) as desired. A few structures in the vesicular component are only hinted at in the original sequence.

In this biological experiment, we focus on the pairwise co-localization of membrane (or vesicular) signals of two pairs of Rab proteins: (Rab8 and Rabin8) and (Rab11a and Rabin8). In Fig. 5 (left), co-localization of (Rab8 and Rabin8) is measured near the plasma membrane of the cell; (Rab11a and Rabin8) appear more co-localized in the same area, for the time scale we considered in this experiment. It turns out that our signal decomposition enables to better assess co-localization for moving and static structures in the image sequences. Each

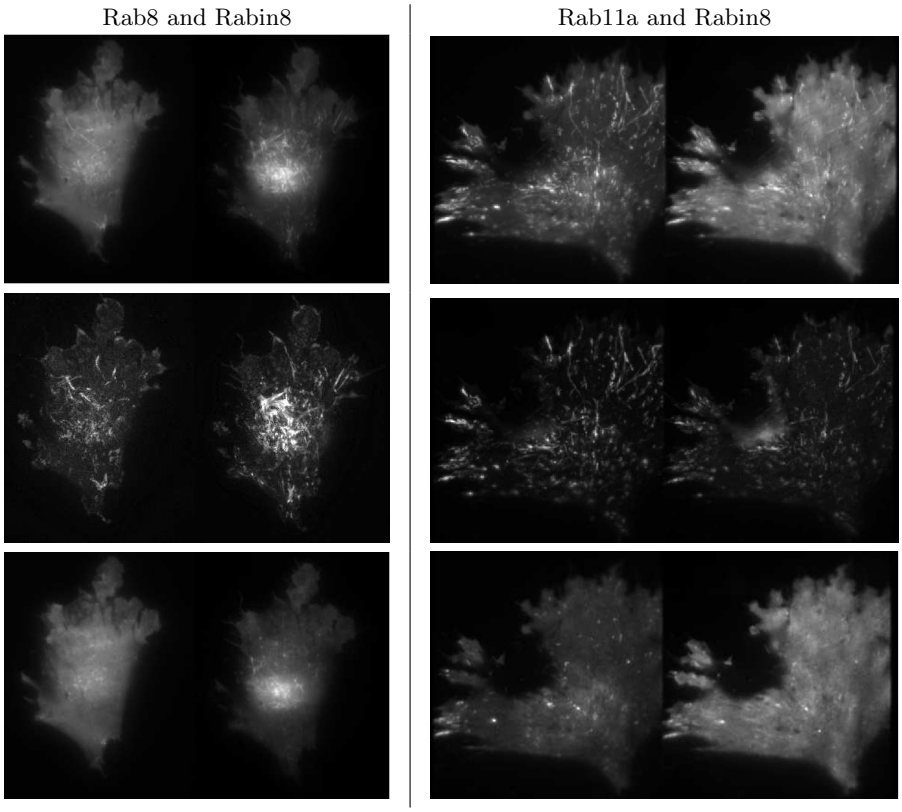

Fig. 5. MIP maps of image sequences. Top to bottom: original images, vesicular components, cytosolic components (see text).

temporal signal is processed individually but the resulting image sequences are surprisingly regularized. While the results are quite preliminary and need to be carefully inspected by experts, we have now the opportunity to perform quantitative spatio-temporal co-localization. This validation is currently underway. It is worth noting that the proposed algorithm is very fast (a few seconds to process several hundred images) and easy to control. It is routinely used by biologists (via the ImageJ software) to separate the membrane (or vesicular) and cytosolic states of Rab proteins. This method is relevant to elucidate the roles of different molecular partners and can be used in many other topics. It will allow further a better description and classification of complex behaviors of various proteins, more reliably than previously, that is from the original image sequences.

5 Conclusion

The computational geometry concepts, earlier introduced for 3D image synthesis were exploited to derive an original scale-space-based signal/image representation. Sub-samplings of the original function are performed, keeping only the

points with enough space around them. The selected points are then used to compute a continuous approximation of the original function by interpolation. The relationships with the Empirical Mode Decomposition was established, since they share algorithmic similarities and enable to represent the original signal using a limited number of modes. The relationships between the proposed framework and several classical scale-space frameworks were also studied. In particular, it was shown that, for a well chosen interpolation operator, the lower α- scale-space is equivalent to a gray-scale opening in mathematical morphology.

Finally the particular case of additive decomposition in video sequences acquired by fluorescence microscopy was addressed and served as a demonstration. The convexity-based decomposition is particularly well suited to the biophysical properties of the studied proteins in fluorescence microscopy.

A number of theoretical questions remain open for investigation. In particular, going beyond spheres to define α-shape, toward α-shapes in generic image-induced metric may lead to interesting results both in theory and practice. Finding an appropriate interpolation operator remains an open question to be addressed in future work.

References

1. I. Amidror. Scattered data interpolation methods for electronic imaging systems: a survey. *Journal of Electronic Imaging*, 11:157–176, April 2002.
2. CGAL Editorial Board. *CGAL-3.2 User and Reference Manual*. 2006.
3. T Bobach, M Hering-Bertram, and G Umlauf. Comparison of voronoi based scattered data interpolation schemes. Palma de Majorque, 2006.
4. J. Boulanger, C. Kervrann, and P. Bouthemy. Estimation of dynamic background for fluorescence video-microscopy. In *Image Processing, 2006 IEEE International Conference on*, pages 2509–2512, 2006.
5. F. Cao. *Geometric curve evolution and image processing*. Springer Lecture notes in mathematics, 2003.
6. V. Caselles, J.M. Morel, and C. Sbert. An axiomatic approach to image interpolation. *IEEE Trans. Image Processing*, 7:376–386, 1998.
7. M. de Berg, M. van Kreveld, M. Overmars, and O .Schwarzkopf. *Computational geometry: algorithms and applications*. Springer-Verlag New York, Inc., Secaucus, NJ, USA, 1997.
8. H. Edelsbrunner and E.P. Mucke. Three-dimensional alpha shapes. *ACM Transactions on Graphics*, 13:43–72, 1994.
9. P. Flandrin, G. Rilling, and P. Goncalves. Empirical mode decomposition as a filter bank. *Signal Processing Letters, IEEE*, 11:112–114, 2004.
10. N. E. Huang, Z. Shen, S. R. Long, M. C. Wu, H. H. Shih, Q. Zheng, N.-C. Yen, C. C. Tung, and H. H. Liu. The empirical mode decomposition and the Hilbert spectrum for nonlinear and non-stationary time series analysis. *Royal Society of London Proceedings Series A*, 454:903, March 1998.
11. J. C. Nunes, Y. Bouaoune, E. Delechelle, O. Niang, and Ph. Bunel. Image analysis by bidimensional empirical mode decomposition. *Image and Vision Computing*, 21:1019–1026, November 2003.
12. J. Panfili, H. de Pontual, H. Troadec, and P.J. Wright, editors. *Manual of fish sclerochronology*. Ifremer-ird coedition, 2002.
13. T. Pecot, C. Kervrann, and P. Bouthemy. Minimal paths and probabilistic models for origin-destination traffic estimation in live cell imaging. In *ISBI 2008*, pages 843–846, 2008.
14. V. Racine, M. Sachse, J. Salamero, V. Frasier, A. Trubuil, and J.-B. Sibarita. Visualization and quantification of vesicle trafficking on a three-dimensional cytoskeleton network in living cells. *Journal of Microscopy*, 225:214–228, 2007.
15. J. Serra. *Image analysis and mathematical morphology. Vol. 1*. Academic press, London ; San Diego ; New York [etc.], 1982.
16. L. Vese. A method to convexify functions via curve evolution. *Commun. Partial Differential Equations*, 24:1573, 1999.